IJC International Journal of Cancer

IJC

International Journal of Cancer

1 JUNE 2010 | VOLUME 126 | NUMBER 11 | WWW.INTJCANCER.ORG

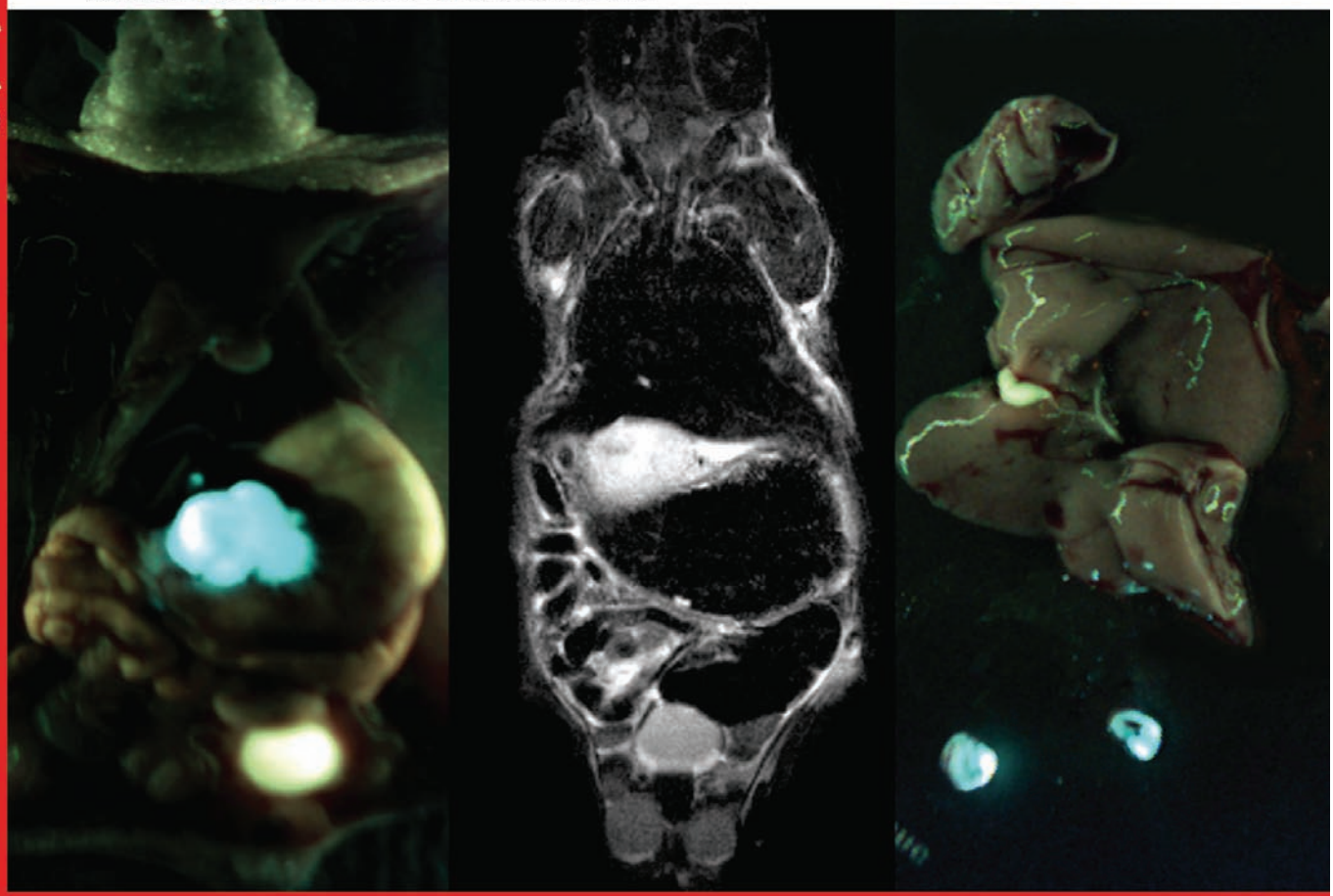

uicc
global cancer control

WILEY-BLACKWELL

www.uicc.org

ISSN 0020-7136

1 JUNE 2010 | VOLUME 126 | NUMBER 11 | PAGES 2511–2758

uicc
global cancer control

IJC
International Journal of Cancer

Complementary use of fluorescence and magnetic resonance imaging of metastatic esophageal cancer in a novel orthotopic mouse model

Stephanie J. Gros[1], Thorsten Dohrmann[1], Kersten Peldschus[2], Paulus G. Schurr[1], Jussuf T. Kaifi[1], Tatyana Kalinina[1], Uta Reichelt[3], Oliver Mann[1], Tim G. Strate[1], Gerhard Adam[2], Robert M. Hoffman[4] and Jakob R. Izbicki[1]

[1] Department of General, Visceral, and Thoracic Surgery, University Medical Center Hamburg-Eppendorf, Hamburg, Germany
[2] Department of Diagnostic and Interventional Radiology, University Medical Center Hamburg-Eppendorf, Hamburg, Germany
[3] Department of Pathology, University Medical Center Hamburg-Eppendorf, Hamburg, Germany
[4] AntiCancer, Inc., San Diego, CA

We describe the development of an aggressive orthotopic metastatic model of esophageal cancer, which is visualized in real time with combined magnetic resonance imaging (MRI) and fluorescence imaging. The aim of the study was to describe the development of a novel model of metastatic tumor disease of esophageal carcinoma and use this model to evaluate fluorescence and MRI in early detection of local and metastatic disease. The human esophageal adenocarcinoma cell line PT1590 was stably transfected with green fluorescent protein (GFP). Nude mice were orthotopically implanted with PT1590-GFP cells. Orthotopic tumor growth as well as metastatic spread was examined by fluorescence imaging and high-resolution MRI at defined intervals after orthotopic implantation. Highly aggressive novel fluorescent cell lines were isolated from metastatic tissues and put into culture. After implantation of these cells, 100% of the animals developed orthotopic primary tumors. In 83% of animals, metastatic spread to liver, lung and lymph nodes was observed. Primary tumor growth could be visualized with fluorescence imaging and with MRI with high correlation between the 2 methods. Fluorescence imaging allows fast, sensitive, and economical imaging of the primary and metastatic tumor without anesthesia. With MRI, anatomical structures are visualized more precisely and tumors can be more accurately localized to specific organs. This model should prove highly useful to understand esophageal carcinoma and to identify novel therapeutics for this treatment-resistant disease.

Esophageal carcinoma is one of the most common cancers in the world and, especially in the advanced stages, a leading cause of death. In the early stages, surgical resection is the only successful treatment. Survival is, however, mostly related to lymph node or distant organ metastases, and there is no effective therapeutic target for successfully treating metastasis. Therefore, understanding metastatic pathways and developing treatment options to reduce the size of the primary tumor and to treat or prevent metastatic spread is of greatest importance.

Orthotopic models made by implanting histologically intact human tumor tissue into mice develop the local and metastatic behaviours occurring in human patients.[1–4] However, a metastatic orthotopic model of esophageal adenocarcinoma, which resembles the aggressive behavior in human disease, has not been established. Lack of such a model has been an impediment for the discovery and development of effective therapeutics for metastatic esophageal cancer.

In addition, accurate and reproducible tumor imaging of orthotopic models can monitor the efficacy of novel therapeutics in real time. Multiple imaging techniques have been applied to small animal imaging. Previously, computed tomography, abdominal ultrasound and magnetic resonance imaging (MRI) have been used. A variety of newer imaging modalities such as *in vivo* fluorescence and bioluminescence imaging have now been established.[1–4] In addition, high-resolution MRI with 3-dimensional reconstruction of image data can provide detailed anatomical information in small rodents.[5] A high correlation of *in vivo* fluorescence imaging and MRI has been shown for pancreatic cancer.[6]

The aim of the study was to first create a reliable orthotopic model of esophageal cancer with a clinically relevant metastatic pattern and to develop a real-time imaging of the chronology of primary tumor growth, progression and development to specific organs in this model.

Orthotopic tumor growth and a clinically relevant metastatic pattern are essential to understand the pathophysioloy of tumor disease and progression, especially in metastic

Key words: orthotopic implantation, esophageal carcinoma, *in vivo* fluorescence imaging, magnetic resonance imaging
DOI: 10.1002/ijc.24980
History: Received 16 Sep 2009; Accepted 13 Oct 2009; Online 21 Oct 2009
Correspondence to: Stephanie J. Gros, Department of General, Visceral, and Thoracic Surgery, University Medical Center Hamburg-Eppendorf, Martinistr. 52, 20251 Hamburg, Germany, Fax: +49-40-42803-4995, E-mail: sgros@uke.uni-hamburg.de

Table 1. Experimental setup

Experimental setup			
Experimental Series I	Subcutaneous model	100% tumor take rate, 0% metastatic rate	Data not shown
	Orthotopic model	100% tumor take rate, 80% metastatic rate	Group 1
Experimental Series II	Fluorescence/MR Imaging	Comparison of modalities	Group 2

Series I was conducted to establish a reliable tumor model for esophageal carcinoma. Series II was conducted to evaluate the impact of fluorescence and MR imaging in this tumor model.

esophageal carcinoma, where few treatment options are available.

The combination of MRI and fluorescence imaging in an orthotopic model demonstrates a powerful approach to the visualization of primary and metastatic spread of esophageal cancer and for the discovery of effective drugs for this treatment-resistant cancer.

Material and Methods

Experimental outline

This study includes 2 series of experiments. Series I was conducted to establish a reliable tumor model for esophageal carcinoma. Series II was conducted to evaluate the impact of fluorescence and MRI in this tumor model (Table 1).

In series I, mice were injected subcutaneously with GFP-PT1590 cells. After 10 weeks all mice all developed subcutaneous tumors. Mice were sacrificed and autopsy performed. However no metastatic tumor growth was visible macroscopically or by *in vivo* fluorescence imaging (data not shown).

GFP-PT1590 tumor fragments were then orthopically implanted to the abdominal esophagus as described below. To evaluate primary tumor growth and metastases, mice were examined every other day until their general performance status decreased, leading to a different experimental end point for each animal. Fluorescence imaging was performed every other day. MRI and open fluorescence imaging were performed at time of autopsy. Evaluation further included histological analysis as gold standard, ex vivo imaging, fluorescence microscopy and GFP-reverse transcriptase PCR (group 1).

In series II, GFP-PT1590 tumor fragments were orthopically implanted to the abdominal esophagus. For comparison of *in vivo* imaging modalities, primary orthotopic tumor growth and metastatic spread were monitored every day by *in vivo* fluoresence imaging and every third day by MRI starting on day 5 after implantation. This series ended on day 55 after orthotopic implantation with final *in vivo* fluorescence and MRI, autopsy, open fluorescence imaging and ex vivo fluorescence imaging (group 2).

Tumor model

Cell lines. The human cell line PT1590 was isolated from a primary tumor of a patient with human esophageal adenocarcinoma at the University Medical Center Hamburg-Eppendorf as previously described.[7,8] Cells were cultured in RPMI 1560 medium (Biochrome KG, Berlin, Germany) containing 10% fetal bovine serum (Linaris, Wertheim-Bettingen, Germany), penicillin/streptomycin (Biochrome KG, Berlin, Germany), transferrin (Sigma-Aldrich, Munich, Germany), insulin (Sigma-Aldrich), basic fibroblast growth factor (Boehringer, Mannheim, Germany) and epidermal growth factor (Boehringer).

Injection and implantation of esophageal carcinoma cell lines. NMRI/nu (U.S. Naval Medical Research Institute) mice were obtained from Charles River Deutschland (Sulzfeld, Germany) at 10 weeks of age and housed in the animal facility of the University Medical Center Hamburg-Eppendorf. All animal procedures were performed in accordance with a protocol approved by the Behörde für Wissenschaft und Gesundheit (Freie und Hansestadt Hamburg, Germany). Cells were harvested after trypsinization and washed 3 times with medium. A total of 5×10^6 GFP-PT1590 fluorescent esophageal adenocarcinoma cells in a 200-µl suspension were subcutaneously injected into the flanks of nude mice with a 1-ml syringe (BD Plastipak, Becton Dickinson S.A., Spain) with a 27-gauge hypodermic needle (Sterican, Braun, Germany) within 40 min of harvesting. Six mice were used (Group 1). Mice were weighed and examined for tumor development every other day. When tumor growth reached 0.6–0.8 cm tumors were excised. Four 1 mm^3 sized esophageal tumor fragments derived from these tumors were orthotopically implanted in the abdominal esophagus of 6 mice for each cell line. Mice were anaesthetized with ketamine hydrochloride (Graeub, Bern, Switzerland)/xylazine hydrochloride (Bayer, Leverkusen, Germany) mixture (12 mg/1.6 mg per ml) and intraperitoneally injected with 10 ml/kg body weight. A 0.8-cm transverse incision of the skin was made in the epigastric abdomen. Abdominal muscles and peritoneum were separated by sharp dissection, and the abdomen was opened. The great curvature of the stomach was held by a forceps, and the liver was raised to expose the abdominal esophagus. A lesion of the esophageal serosa was made with a sharp forceps. Tumor fragments were sewn in this lesion with an 8.0 prolene suture (Ethicon, Norderstedt, Germany). The incision of the abdominal wall was closed using 6.0 vicryl sutures (Ethicon, Norderstedt, Germany). All procedures of the operation, as described above, were performed under an operating microscope (Carl Zeiss, Jena, Germany). Postoperative

analgesia was achieved by novamine sulfone (1 mg/ml) in drinking water. Mice were weighed and examined for tumor development every other day. Furthermore, this procedure was repeated on 6 mice for combined MRI and *in vivo* fluorescence imaging (group 2).

Imaging

Fluorescence imaging

Transfection of esophageal carcinoma cells with green fluorescent protein. PT1590 cells were transfected with pEGFP-N1 and pLEGFP-N1 plasmids (Clontech, Palo Alto, CA). To select clones with resistence to neomycin, neomycin was added after transfection. The dose of neomycin was increased in a stepwise manner. GFP expression was monitored by fluorescence microscopy. Cells were isolated and cultivated at 37°C in a 5% CO_2 incubator.

In vivo fluorescence imaging. Mice were monitored daily by noninvasive *in vivo* fluorescence imaging using a Pan-a-see-ya panoramic imaging system® (Lightools Research, Encinitas, CA) with fiberoptic lighting at 490 nm. No anaesthesia was necessary to perform routine imaging. To improve the quality of images, mice were occasionally anaesthetized with carbondioxide for a few seconds. Images were processed for contrast and brightness using Adobe® Photoshop.

At the time of sacrifice, open fluorescence imaging was performed. Primary tumor and mestastic spread could be visualized and organ localization could be confirmed. After whole body imaging, the organs and lymph nodes were dissected and removed to be examined further for metastasis using fluorescence imaging.

Magnetic resonance imaging

Whole body MRI of tumor-bearing mice was performed under anesthesia with ketamine hydrochloride/xylacine hydrochloride as described above. High-resolution magnetic resonance (MR) data sets were acquired on a clinical 3-Tesla whole body MR scanner (Intera, Philips Medical Systems, Best, the Netherlands) equipped with a standard gradient system (gradient strength = 40 mT/m). A dedicated small animal solenoid receiver coil (Philips Research, Hamburg, Germany) with an inner diameter of 40 mm and an integrated heating system to regulate body temperature of mice during MR scans was used for signal acquisition. The MR protocol consisted of a short survey scan and 3 T2-weighted 2-dimensional turbo spin-echo sequences in coronal, sagittal and axial orientations. Imaging parameters were as follows: repetition time = 2674 msec; echo time = 90 msec; echo train length = 10, number of excitations = 2. The acquisition matrix and field-of-view (FOV) were adopted to display the animals in each orientation with an in-plane resolution of 200 × 200 μm. For coronal and sagittal images, a matrix of 400 × 200 pixels and a FOV of 80 × 40 mm were used. Axial images were acquired with a matrix of 160 × 128 pixels and a FOV of 32 × 25.6 mm. Slice parameters were equal for all 3 sequences with a thickness of 800 μm and 14 slices. The total scan time per animal was 10 min 42 sec. Image processing and analysis were done on a conventional clinical workstation by a clinical radiologist (K.P.) in accordance with the clinical standards. Suspicious lesions were considered primary tumors or metastatic tumors if they appeared hyperintense on the T2-weighted images and had a diameter ≥1 mm.

Comparison of imaging modalities

Comparison of fluorescence imaging and MRI. Both fluorescence and MRI on tumor-bearing mice were performed repeatedly over time. While fluorescence imaging was performed daily, MRI was started on Day-4 after tumor implantation and repeated with an interval of 3 days. MRI requires anaesthesia and as thus stress as well a possible risk of reaction to narcotics. It also might cause interference with treatment regimens the mice may be subjected to. To allow postoperative recovery, MRI was started only on day 5 and to allow recovery from anesthesia, MRI was performed every 3 days thereafter. Observations were concluded on Day-55.

The individual tumor burden was measured by determination of the maximum diameter of lesions by MRI and fluorescence imaging. Image analysis was performed on a conventional clinical workstation by a clinical radiologist (K.P.). The minimal distance of tumors to the abdominal wall was recorded at each time point and correlated to the time of the initial presence of fluorescence determined by noninvasive imaging.

Evaluation

Primary tumor. When the performance status of the mice decreased because of tumor progression, the animals were killed and autopsied. The orthotopic primary tumor as well as lung, liver, axillary, mediastinal, paraesophageal, mesenteric and inguinal lymph nodes were dissected and examined with the fluorescence imaging system. Fragments of metastatic liver, lung and lymph node that were visible using the Lightools imaging system were placed into Hank's solution for further preparation of metastatic cell lines. The remaining tissue was cryopreserved.

Metastases

H.E. staining and light microscopy. Cryosections were fixed and stained by standard H&E staining. Examination was performed by light microscopy (Olympus C3030, Hamburg, Germany) by 3 independent examiners (S.G., T. D. and U.R.).

Fluorescence microscopy of GFP-esophageal carcinoma. Fluorescence microscopy was performed using a fluorescence microscope (Leica, Solms, Germany) with 480 nm filter set. Frozen sections of all tissues were prepared with a cryotome (Microm HD550, Walldorf, Germany) and immediately examined for GFP fluorescence by 2 independent examiners (S.G. and T. D.).

RNA extraction and GFP-amplification. Primary and metastatic GFP-cells were harvested after trypsinization and washed 3

Table 2. Primary tumor growth and metastatic pattern of orthotopically implanted PT1590 human esophageal cancer

Mouse	Survival time (days)	Weight (g)	Primary tumor weight (g)	Metastasis		Lymph node Involvement
				Liver	Lung	
1	56	36.9	6.8	+	+	−
2	31	29.5	5.4	+	+	+
3	30	30.8	2.3	−	+	+
4	71	25.5	5.6	+	+	+
5	71	29.7	5.7	−	−	+
Overall	41.8	30.48	5.16	60%	80%	80%

Nude mice were implanted with tissue fragments of human PT1590 esophageal adenocarcinoma expressing GFP. Metastases were determined by GFP imaging and MRI. Table 1 summarizes survival time, weight of the mice and primary tumor at time of autopsy as well as overall metastatic spread for experimental Group 1. Metastatic spread to liver, lung and lymph nodes was seen in 60, 80 and 80%, respectively.

times. A total of 5 x 10^6 cells were used for RNA extraction using the PARIS® Kit (Ambion, Austin, TX). Representative tissue of liver, lung, lymph node and primary tumor was mechanically homogenized using a MediMachine® (DakoCytomatation, Hamburg, Germany). Homogenized lysate was used for RNA extraction using the PARIS® Kit. cDNA was obtained with a Invitrogen rtPCR (reverse transcriptase polymerase chain reaction) kit®. Amplification of GFP DNA was performed with Thermocycler (Biometra, Göttingen, Germany) with a Taq-Polymerase (Roche, Mannheim, Germany) and GFP-specific primer (GTAAACGGCCAAGTTCAG, AGCTCGATGCGGTTCACCAG). PCR products were run on a 2% agarose gel. Imaging was performed with a Biodoc II™ (Biometra, Göttingen, Germany). For size reference, a 100-bp DNA ladder (New England Biolabs, Frankfurt, Germany) was used. Experiments were performed twice.

Isolation of metastatic cell lines

Fresh tumorous tissue (liver, lung and lymph nodes) that showed GFP fluorescence was divided under sterile conditions into 1 mm small pieces and mechanically disaggregated in 2 ml RPMI 1560 medium using a MediMachine® (DakoCytomatation). The cell suspension was placed in a 25-cm^2 cell culture bottle flask with RPMI 1560.

Results

Tumor model

Isolation of stable GFP-expressing esophageal carcinoma cells. GFP-transfected PT1590 esophageal adenocarcinoma cells were capable of growing *in vitro* under neomycin selection. The selected neomycin-resistant carcinoma cells exhibited bright GFP fluorescence *in vitro* (data not shown).

Subcutaneous tumor growth with GFP expression. Six days after implantation, visible subcutaneous tumor growth of PT1590-GFP was observed in 100% of the implanted animals. After 3 weeks, GFP-PT1590 tumors had reached 0.6–0.8 cm and were harvested for orthotopic implantation. On autopsy of the subcutaneously implanted mice, there was no tumor spread detectable by fluorescence imaging.

Orthotopic primary tumor growth with GFP expression. All 12 mice in Groups 1 and 2 (100%) developed orthotopic tumor growth after implantation with PT1590-GFP tumor fragments. Survival times and tumor weights for Group 1 are summarized in Table 2. One animal died from total colonic necrosis most likely not related to orthotopic tumor development (mouse 3). Beginnning 14 days after implantation, mice implanted with GFP-PT1590 cells demonstrated GFP fluorescence from the orthotopically-implanted tumor in the abdominal esophagus. At the time of initial detection of tumor fluorescence, there was neither a palpable abdominal tumor at the implantation site nor a decrease in the general performance status of the mice. At this time, 3 of 5 mice had GFP fluorescence from the liver and one from the left lung (Fig. 1*a*). Tumor location in the abdominal esophagus could be demonstrated by *in vivo* MRI by 2 weeks after implantation. Mice (Group 1) were killed when their general performance status decreased between weeks 5 and 10 postoperatively. Throughout, there was no difference in body weight of the tumor-bearing mice and control mice not implanted with tumor (data not shown).

Metastases expressing GFP. On autopsy, the primary tumors at the site of implantation were attached to the serosa of the abdominal esophagus. Open imaging of mice in Group 1 confirmed GFP-expressing cells in the liver in 3 mice and in the lung in 2 mice, as well as 2 GFP-positive lymph nodes in 1 mouse and 3 GFP-positive lymph nodes in another mouse. (Fig. 1*c*; Fig. 2*a* and 2*b*). Orthotopic tumor growth and metastases were confirmed by fluorescence and light microscopy of cryosections (Fig. 1*b* and 1*c*).

The tissue was divided and partially used for cell culture. Fluorescence and light microscopy of cryosections of remaining tissue confirmed metastasis in the liver (40%), lung (40%) and lymph nodes (60%). The presence of GFP-positive cells in potential metastastic tissues was confirmed by reverse transcriptase PCR (Fig. 2*c*). Tissues taken for homogenization

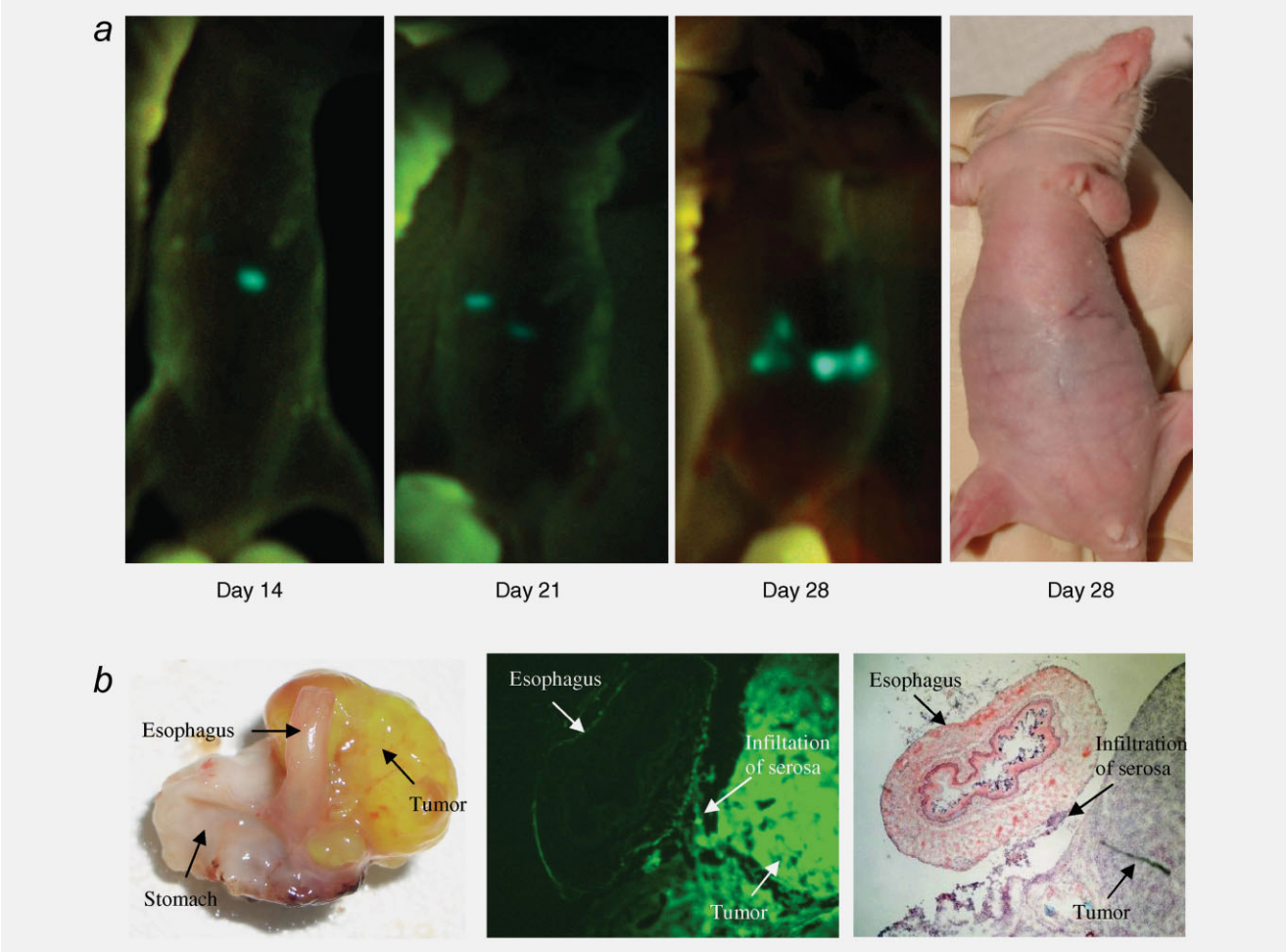

Figure 1. Whole body imaging of mouse 2 (Group 1) with the fluorescence imaging system demonstrates a green fluorescent protein signal visible 14 days after orthotopic implantation to the abdominal esophagus (*a*). After 21 days, there was a second GFP signal visible from the liver, and after an additional week, there was definite progression in tumor size and intensity of fluorescence. After 28 days, the mouse was still alive and without visible tumor under normal lighting. Necropsy of the primary tumor at the abdominal esophagus (*b*). Fluorescence microscopy and H.E. staining confirm tumor infiltration of the esophageal serosa.

and rt-PCR showed metastases to the liver in 20%, to the lung in 80% and to the lymph nodes in 80% (Fig. 2*d*), allowing the conclusion that overall metastatic spread occurred in 60% to the liver and in 80% to lung and lymph nodes (Table 3).

Establishment of novel metastatic cell lines. Metastatic cell lines could be established from the primary orthotopic tumor, from liver and lung metastatic tissue as well as from mesenteric, mediastinal and paraesophageal lymph nodes of 4 mice. Metastatic cell lines showed strong GFP fluorescence *in vitro*, demonstrating stable high-level GFP expression.

Imaging

Primary tumor

Comparison of whole body fluorescence imaging and MRI of primary esophageal tumors. Six mice were used to compare imaging modalities after orthotopic implantation of esophageal adenocarcinoma (group 2). One mouse died on day-7 because of reaction to intraperitoneal anesthesia administered for MRI and was therefore excluded from further evaluation. Sequential MRI and fluorescence imaging was started at Day 4 after orthotopic implantation and showed development of tumor growth over time. The orthotopic esophageal tumor in all mice was visible by MRI by Day 18. The maximum diameter of the tumor was used as the parameter for tumor growth.

After Day 21, the fluorescent primary tumor was clearly visible by both imaging modalities, and its size seen by T2-weighted MRI and fluorescence imaging correlated well with the actual tumor size at the time of autopsy (Fig. 3). Tumor growth after Day-14 was consistently progressive (Fig. 4*a*).

Noninvasive fluorescence imaging was limited by the minimum distance of the tumor to the abdominal wall of the mouse in frontal and side view imaging. In this study, we found that tumors that were >4.2 mm from the abdominal wall could not be distinguished by fluorescence imaging.

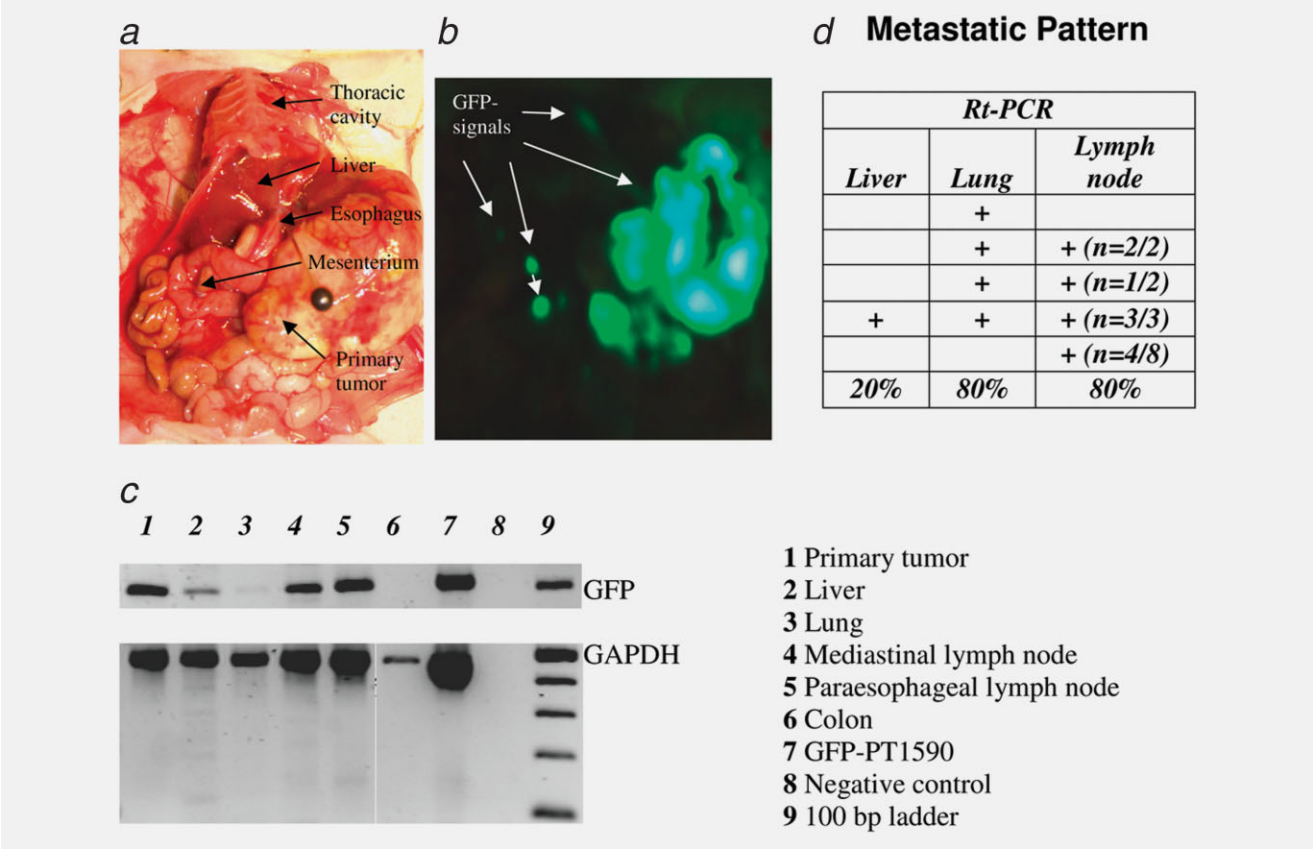

Figure 2. Open fluorescence imaging at time of autopsy reveals GFP fluorescence in left lung, liver and at 2 sites of mesenterium (*a*,*b*). Reverse transcriptase PCR shows presence of GFP mRNA in mouse 5 in the primary tumor, liver, lung, mediastinal and paraesophageal lymph nodes as well as in the PT1590-GFP cell line positive control. The mouse colon is free of cells containing GFP mRNA (*c*). rt-PCR shows the highest sensitivity. (+) indicates a positive result.

Table 3. Comparison of methods for metastatic detection

	In vivo imaging			H.E.staining			Fluorescence microscopy *ex vivo*		
Mouse	Liver	Lung	Lymph node	Liver	Lung	Lymph node	Liver	Lung	Lymph node
1	+	+		+	+		+	+	
2	+		+(n=2/2)			+(n=3/5)			+(n=3/5)
3									
4	+	+	+(n=3/3)	+	+	+(n=4/4)	+	+	+(n=4/4)
5						+(n=10/4)			+(n=10/4)
Overall	60%	40%	40%	40%	40%	*60%*	40%	40%	40%

Methods were compared to detect PT1590 metastases after orthotopic transplantation as in Table 1. See Material and Methods for details.

Measurements were also obtained noninvasively by MR scanning (Fig. 4*b*).

Metastases

Comparison of fluorescence imaging and MRI of metastatic tumors. Although MR images provide a more detailed view of anatomical structures, fluorescence imaging provides a highly specific signal of primary and metastastic tumor growth. Open fluorescence imaging allows a more detailed view of internal organs and metastases that are found >4.2 mm from the abdominal wall (Fig. 4*b*). Lymph node metastases in group 2 were observed in 80%, and liver metastases in 40%, of the mice by fluorescence imaging alone. Positive lymph nodes included the mesenteric, coeliac, paraesophageal and axillary lymph nodes. Neither lymph node metastases nor small liver metastases were visible with MRI.

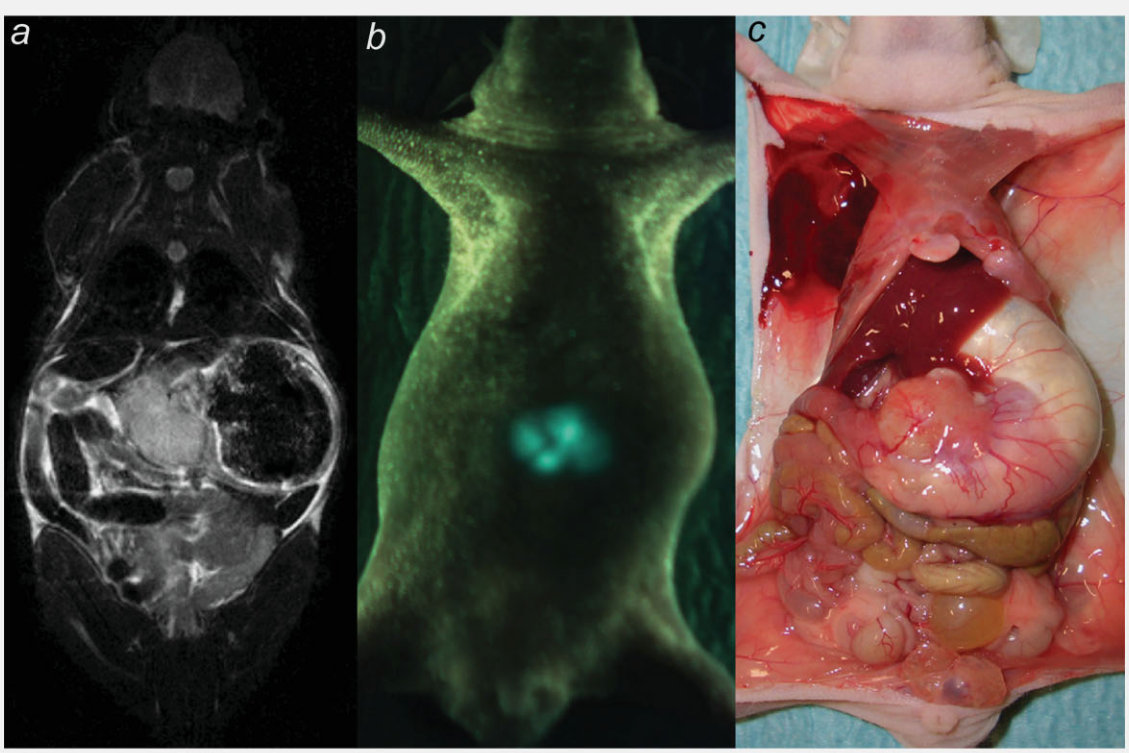

Figure 3. Visualization of primary esophageal tumor by T2-weighted MRI (*a*) and fluorescence (*b*) imaging correlates with the orthotopic site of implantation and the abdominal esophagus at time of sacrifice. Sequential T2-weighted MR and fluorescence images were obtained over the course of development of fluorescent PT1590-GFP esophageal tumors. Tumor was clearly visible by both imaging modalities and correlates with tumor size in open images (*C*).

In some cases, fluorescence imaging was in some cases limited by superimposition of internal organs, which did not allow the fluorescence signal to be registered. In the present model of abdominal esophageal carcinoma, noninvasive imaging of progressive disease was found to be obstructed especially by the stomach and the liver overlying the primary tumor. In these cases, MRI however could provide anatomical identification of superimposed organs and could more precisely visualize the outline of the primary tumor (Fig. 4*c* and 4*d*).

Lymph nodes and organs were dissected at the time of sacrifice and examined separately. Imaging allowed highly specific visualization of tumor tissue. Metastases in tissues that *in vivo* were superimposed by primary tumor could be identified by *ex vivo* fluorescence imaging allowing detailed examination of all organs, including lymph nodes (Fig. 4*e*) and the liver (Fig. 4*d*).

Discussion

In our novel mouse model of orthotopic esophageal adenocarcinoma, local tumor growth was reproducibly seen in 100% of cases after implantation of PT1590-GFP cells. It is crucial to investigate the biology of the primary tumor as well as that of metastatic targeting for esophageal carcinoma because the treatment of esophageal carcinoma is still limited by the stage at initial diagnosis and surgical resectability. Currently, there is no effective chemotherapeutic or biological treatment for metastatic esophageal cancer.

The unique cell PT1590 line was generated at the University Medical Center Hamburg-Eppendorf from the primary tumor obtained from a patient with esophageal cancer classified as stage pT1pN1M0 according to the tumor-node-metastasis classification of the International Union Against Cancer.[9] The lymph node was classified as tumor free by routine histopathological methods (hematoxylin and eosin staining), but it contained 3 Ber-Ep4-positive cells per approximately 10^5 lymph node cells,[8] indicating micrometastatic spread in this lymph node. The tumorigenic potential of the LN1590 cell line has previously been described.[10] However, it has not been possible in these studies to establish a metastatic spreading pattern analogous to that in humans in mice by subcutaneous injection of tumor cells alone.

Orthotopic models have been established for numerous tumor entities.[11] Metastastatic spread has been observed to be enhanced after orthotopic implantation of human cells. Human colon cell line suspensions injected into the cecum of nude mice eventually led to metastasis to the liver, as would be expected in human colorectal cancer.[12–18] Similar orthotopic mouse models have been developed for human lung carcinoma,[19,20] stomach carcinoma,[21–23] bladder

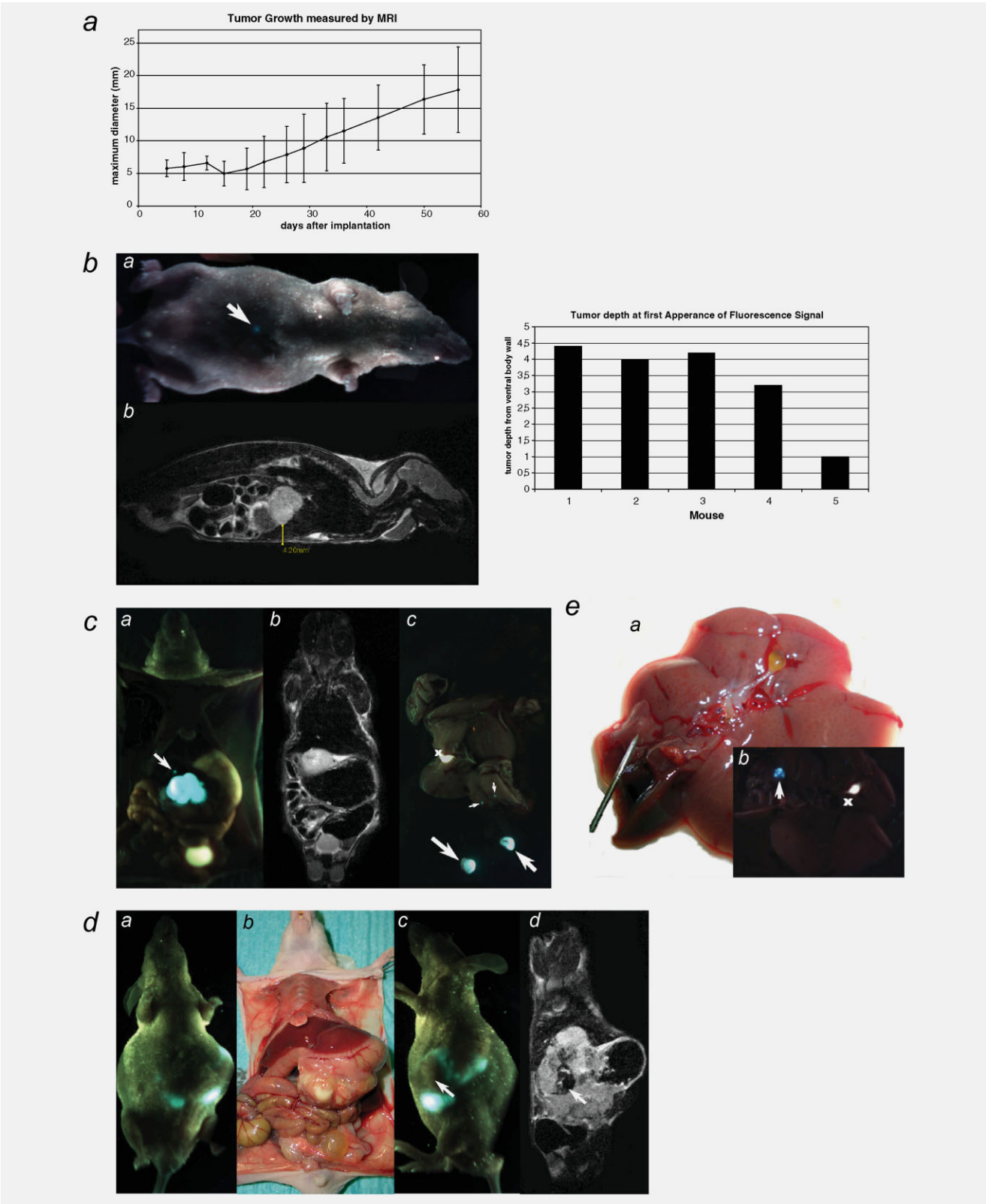
a
Tumor Growth measured by MRI
maximum diameter (mm)
days after implantation
b
a
b
4.20mm
Tumor depth at first Apperance of Fluorescence Signal
tumor depth from ventral body wall
Mouse
c
a
b
c
e
a
b
d
a
b
c
d

Figure 4.

cancer,[21,24–26] melanoma,[21,27,28] breast cancer[21,29–33] and head and neck cancer.[34]

It has been shown for other tumor entities that orthotopic implantation is a key method to achieve reliable primary growth and metastatic spread. Orthotopic models of pancreatic tumor have however demonstrated tumor take rates of 100% and metastatic rates of 40%[35] with metastases to regional and distant lymph nodes and to the liver and lung.[36] A model of squamous cell carcinoma of the cervical esophagus in rats achieved 99.5% tumor take with 3 lymphatic micrometastases in 22 rats.[37] In an inoculation model of squamous cell carcinoma of the esophagus, metastasis was not detectable, although primary tumor growth was substantial.[38]

In our novel orthotopic tumor model of esophageal carcinoma, implanted mice developed metastases in 100% of the animals, whereas in the subcutaneously implanted group, 100% of animals showed subcutaneous tumor growth without metastatic spread. In the orthotopic model, there was metastatic spread to the liver in 60% of the mice and to the lung and lymph nodes in 80% of mice, demonstrating that this model has very high metastatic potential. Moreover, we have been able to cultivate metastatic cell lines from liver, lung and lymph node metastases, which as the primary cell line highly express GFP. Metastases in all mice could be verified by at least 2 of 3 methods we used (Table 2, Fig. 1*c* and Fig. 2*d*). As expected, rt-PCR overall showed the highest sensitivity. The location of the orthotopic primary tumor could be visualized by highly sensitive small animal MRI. Visualization of metastatic spread in MRI however still needs improvement, e.g., using breathing and electrocardiographically triggered imaging to restrict artifacts and increase sensitivity of metatastatic imaging.

Fluorescence imaging allows highly specific visualization of primary tumor and metastatic spread in the orthotopic model of esophageal carcinoma. Imaging is easily obtained without any contrast agent or anesthesia. The fluorescence imaging technique is simple to use and inexpensive. Serial imaging is highly reproducible, and tumor progression can be visualized accurately. Furthermore, the fluorescence imaging technique is animal friendly. However, fluorescence imaging is limited by the distance of the tumor from the abdominal wall.

Open fluorescence imaging with selective imaging of specific organs allows visualization of small metastases, especially of liver, lung or lymph node metastases that could not be detected by whole body imaging because of their size or their depth. The short image acquisition time allows rapid visualization without anaesthesia during scanning.

High-resolution MRI allows morphological evaluation of primary tumors and metastases. It facilitates visualization of the individual anatomy as well as localization and delineation of the tumor. Hence, an accurate assessment of the size and intraperitoneal depth of tumors is possible. We found the increase of tumor size determined by MRI to be unspecific during the first 2 weeks after tumor implantation, but slightly more sensitive than fluorescence imaging after Day 18. Although the sensitivity of detection of the primary tumor is high, MRI without contrast agents in the setup described here is not sensitive enough to visualize metastases of small dimensions, such as in lymph nodes.[39,40] A thorough imaging of the lungs due to air artifacts is inhibited by the longer image acquisition time needed in our setup. Furthermore, the need to immobilize the animals require general anesthesia during MR scanning. MR scanners at higher field strengths, such as 7 T or 9.4 T, may improve sensitivity to detect small metastasis.[41]

An approach of combining fluorescence and MRI enables serial high-resolution images to be acquired. *In vivo* imaging of live animals with fluorescence imaging is efficient, inexpensive, animal friendly and highly specific for primary

Figure 4. (*a*) Sequential MRI shows tumor growth over time. The maximum diameter of the tumor was used as the parameter for measurement of tumor growth (*a*). Imaging was initially performed at Day 3 after orthotopic implantation. During the first 12 days, an increase in diameter was observed, which regressed by Day 15. Following Day 15, a consistent increase in diameter was recorded. During the first 12 days, inflammatory reaction in tumor-surrounding tissue may be responsible for the measured increase in tumor diameter. (*b*) Fluorescence imaging was performed with the Lightools® imaging unit. Frontal and side views were obtained (*b*). In this single mouse, a minimum distance of the tumor from the abdominal wall of 4.2 mm was measured in MRI at the time of first appearance of fluorescence signal. (*c*) Open fluorescence imaging allows a more detailed view of internal organs as well as metastases. Next to the strong fluorescence signal of the primary tumor, an additional fluorescence signal, indicated by the arrow, is visible in open imaging (*a*). The signal colocalizes with the location of a coeliac lymph node. Although MRI (*b*) allows well-defined visualization of primary tumor, the coeliac lymph node metastasis (indicated by arrow in *a*) as well as the positive mesenteric and axillary lymph nodes and small liver metastases (indicated by arrows in *c*) can only be visualized by fluorescence imaging. (*d*) Frontal view of mouse in fluorescence imaging (*a*) shows fluorescence tumor signal that is inconsistent with expected size of primary tumor. Open image of mouse (*b*) reveals the tumor to be partially superimposed by the liver and stomach. Comparison of side view fluorescence image (*c*) with sagital plane of MRI (*d*) demonstrates that overlying structures that limit fluorescence imaging can be identified by MRI as stomach and liver, indicated by arrows. (*e*) Diagnosis of liver metastases is visualized by fluorescence imaging. A macroscopically suspicious focus on the liver (*a*) at time of sacrifice can be confirmed as liver metastasis (indicated by arrow) with fluorescence *ex vivo* imaging (*b*).

tumor and metastases, whereas MRI provides accurate organ and tumor anatomy, and allows more precise localization of the tumor.

Conclusion

Implantation of the esophageal carcinoma cell line PT1590-GFP to the abdominal esophagus leads to a 100% tumor take rate. Hundred percent of animals with orthotopic esophageal adenocarcinoma developed metastases with spread to liver in 60% and to lung and lymph nodes in 80% of animals. The local and metastatic aggressiveness of this cancer was further demonstrated by cultivating metastatic cell lines from the primary tumor as well as liver, lung and lymph node metastases, which like the primary cell line highly express green fluorescent protein.

The high correlation of fluorescence imaging and MRI in this orthotopic esophageal model, which exhibits clinical patterns of local and metastatic behaviour as they occur in human esophageal carcinoma, suggests combined use of these complementary imaging modalities in this orthotopic esophageal model for noninvasive screening of novel therapeutics for this disease.

References

1. Hoffman RM. Whole-body fluorescence imaging with green fluorescence protein. *Methods Mol Biol* 2002;183:135–48.
2. Hoffman RM. The multiple uses of fluorescent proteins to visualize cancer in vivo. *Nat Rev Cancer* 2005;5:796–806.
3. Hoffman RM, Yang M. Subcellular imaging in the live mouse. *Nat Protoc* 2006;1: 775–82.
4. Hoffman RM, Yang M. Color-coded fluorescence imaging of tumor-host interactions. *Nat Protoc* 2006;1:928–35.
5. Ittrich H, Lange C, Togel F, Zander AR, Dahnke H, Westenfelder C, Adam G, Nolte-Ernsting C. In vivo magnetic resonance imaging of iron oxide-labeled, arterially-injected mesenchymal stem cells in kidneys of rats with acute ischemic kidney injury: detection and monitoring at 3T. *J Magn Reson Imag* 2007;25:1179–91.
6. Bouvet M, Spernyak J, Katz MH, Mazurchuk RV, Takimoto S, Bernacki R, Rustum YM, Moossa AR, Hoffman RM. High correlation of whole-body red fluorescent protein imaging and magnetic resonance imaging on an orthotopic model of pancreatic cancer. *Cancer Res* 2005;65: 9829–33.
7. Pantel K, Dickmanns A, Zippelius A, Klein C, Shi J, Hoechtlen-Vollmar W, Schlimok G, Weckermann D, Oberneder R, Fanning E. Establishment of micrometastatic carcinoma cell lines: a novel source of tumor cell vaccines. *J Natl Cancer Inst* 1995;87:1162–8.
8. Scheunemann P, Izbicki JR, Pantel K. Tumorigenic potential of apparently tumor-free lymph nodes. *N Engl J Med* 1999;340:1687.
9. Pantel K, Schlimok G, Angstwurm M, Passlick B, Izbicki JR, Johnson JP, Riethmuller G. Early metastasis of human solid tumours: expression of cell adhesion molecules. *Ciba Found Symp* 1995;189: 157–70.
10. Hosch S, Kraus J, Scheunemann P, Izbicki JR, Schneider C, Schumacher U, Witter K, Speicher MR, Pantel K Malignant potential and cytogenetic characteristics of occult disseminated tumor cells in esophageal cancer. *Cancer Res* 2000;60:6836–40.
11. Hoffman RM. Orthotopic metastatic mouse models for anticancer drug discovery and evaluation: a bridge to the clinic. *Invest New Drugs* 1999;17:343–59.
12. Bresalier RS, Raper SE, Hujanen ES, Kim YS. A new animal model for human colon cancer metastasis. *Int J Cancer* 1987;39: 625–30.
13. Bresalier RS, Hujanen ES, Raper SE, Roll FJ, Itzkowitz SH, Martin GR, Kim YS. An animal model for colon cancer metastasis: establishment and characterization of murine cell lines with enhanced liver-metastasizing ability. *Cancer Res* 1987;47: 1398–406.
14. Fidler IJ. Critical factors in the biology of human cancer metastasis: twenty-eighth G.H.A. Clowes memorial award lecture. *Cancer Res* 1990;50:6130–8.
15. Giavazzi R, Jessup JM, Campbell DE, Walker SM, Fidler IJ. Experimental nude mouse model of human colorectal cancer liver metastases. *J Natl Cancer Inst* 1986; 77:1303–8.
16. Giavazzi R, Campbell DE, Jessup JM, Cleary K, Fidler IJ. Metastatic behavior of tumor cells isolated from primary and metastatic human colorectal carcinomas implanted into different sites in nude mice. *Cancer Res* 1986;46(4 Pt 2):1928–33.
17. Morikawa K, Walker SM, Nakajima M, Pathak S, Jessup JM, Fidler IJ. Influence of organ environment on the growth, selection, and metastasis of human colon carcinoma cells in nude mice. *Cancer Res* 1988;48:6863–71.
18. Sordat B, Wang WR. Human colorectal tumor xenografts in nude mice: expression of malignancy. *Behring Inst Mitt* 1984;74: 291–300.
19. McLemore TL, Liu MC, Blacker PC, Gregg M, Alley MC, Abbott BJ, Shoemaker RH, Bohlman ME, Litterst CC, Hubbard WC. Novel intrapulmonary model for orthotopic propagation of human lung cancers in athymic nude mice. *Cancer Res* 1987;47:5132–40.
20. Wang X, Fu X, Hoffman RM. A new patient-like metastatic model of human lung cancer constructed orthotopically with intact tissue via thoracotomy in immunodeficient mice. *Int J Cancer* 1992; 51:992–5.
21. Furukawa T, Kubota T, Watanabe M, Kuo TH, Kitajima M, Hoffman RM. Differential chemosensitivity of local and metastatic human gastric cancer after orthotopic transplantation of histologically intact tumor tissue in nude mice. *Int J Cancer* 1993;54:397–401.
22. Yamashita T. Manifestation of metastatic potential in human gastric cancer implanted into the stomach wall of nude mice. *Jpn J Cancer Res* 1988; 79:945–51.
23. Furukawa T, Fu X, Kubota T, Watanabe M, Kitajima M, Hoffman RM. Nude mouse metastatic models of human stomach cancer constructed using orthotopic implantation of histologically intact tissue. *Cancer Res* 1993;53:1204–8.
24. Ahlering TE, Dubeau L, Jones PA. A new in vivo model to study invasion and metastasis of human bladder carcinoma. *Cancer Res* 1987;47(24 Pt 1):6660–5.
25. Soloway MS, Nissenkorn I, McCallum L. Urothelial susceptibility to tumor cell implantation: comparison of cauterization with *N*-methyl-*N*-nitrosourea. *Urology* 1983;21:159–61.
26. Fu X, Hoffman RM. Human RT-4 bladder carcinoma is highly metastatic in nude mice and comparable to ras-H-transformed RT-4 when orthotopically onplanted as histologically intact tissue. *Int J Cancer* 1992;51:989–91.
27. Kozlowski JM, Fidler IJ, Campbell D, Xu ZL, Kaighn ME, Hart IR. Metastatic behavior of human tumor cell lines grown in the nude mouse. *Cancer Res* 1984;44: 3522–9.
28. Kozlowski JM, Hart IR, Fidler IJ, Hanna N. A human melanoma line heterogeneous with respect to metastatic capacity in athymic nude mice. *J Natl Cancer Inst* 1984;72:913–7.

29. Basolo F, Fontanini G, Squartini F. Differences in progression of BALB/cfRIII and BALB/cfC3H mammary hyperplastic alveolar nodules transplanted into the gland-free fat pads of BALB/c mice. *Cancer Res* 1988;48:3197–202.
30. Miller FR, McInerney D. Epithelial component of host–tumor interactions in the orthotopic site preference of a mouse mammary tumor. *Cancer Res* 1988;48: 3698–701.
31. White AC, Levy JA, McGrath CM. Site-selective growth of a hormone-responsive human breast carcinoma in athymic mice. *Cancer Res* 1982;42:906–12.
32. Fu X, Le P, Hoffman RM. A metastatic orthotopic-transplant nude-mouse model of human patient breast cancer. *Anticancer Res* 1993;13:901–4.
33. Miller FR, Medina D, Heppner GH. Preferential growth of mammary tumors in intact mammary fatpads. *Cancer Res* 1981; 41:3863–7.
34. Dinesman A, Haughey B, Gates GA, Aufdemorte T, Von Hoff DD. Development of a new in vivo model for head and neck cancer. *Otolaryngol Head Neck Surg* 1990;103(5 Pt 1):766–74.
35. Fu X, Guadagni F, Hoffman RM. A metastatic nude-mouse model of human pancreatic cancer constructed orthotopically with histologically intact patient specimens. *Proc Natl Acad Sci USA* 1992;89:5645–9.
36. Vezeridis MP, Doremus CM, Tibbetts LM, Tzanakakis G, Jackson BT. Invasion and metastasis following orthotopic transplantation of human pancreatic cancer in the nude mouse. *J Surg Oncol* 1989;40: 261–5.
37. Hori T, Yamashita Y, Ohira M, Matsumura Y, Muguruma K, Hirakawa K. A novel orthotopic implantation model of human esophageal carcinoma in nude rats: CD44H mediates cancer cell invasion in vitro and in vivo. *Int J Cancer* 2001;92:489–96.
38. Furihata T, Sakai T, Kawamata H, Omotehara F, Shinagawa Y, Imura J, Ueda Y, Kubota K, Fujimori T. A new in vivo model for studying invasion and metastasis of esophageal squamous cell carcinoma. *Int J Oncol* 2001;19:903–7.
39. Harisinghani MG, Barentsz J, Hahn PF, Deserno WM, Tabatabaei S, van de Kaa CH, de la RJ, Weissleder R. Noninvasive detection of clinically occult lymph-node metastases in prostate cancer. *N Engl J Med* 2003;348:2491–9.
40. Kobayashi H, Brechbiel MW. Dendrimer-based nanosized MRI contrast agents. *Curr Pharm Biotechnol* 2004;5:539–49.
41. Baboi LM, Milot L, Lartizien C, Roche C, Scoazec JY, Pilleul F, Beuf O. Characterization of neuro-endocrine tumors in an athymic nude mouse model using dedicated synchronization strategies for T2-weigted MR imaging at 7T. *Conf Proc IEEE Eng Med Biol Soc* 2007;2007: 2879–82.